

# More than one dynamic crossover in protein hydration water

Marco G. Mazza,<sup>1</sup> Kevin Stokely,<sup>1</sup> Sara E. Pagnotta,<sup>2</sup>  
Fabio Bruni,<sup>3</sup> H. Eugene Stanley,<sup>1</sup> and Giancarlo Franzese<sup>4</sup>

<sup>1</sup>*Center for Polymer Studies and Department of Physics,  
Boston University – Boston, MA 02215 USA*

<sup>2</sup>*Centro de Física de Materiales (CSIC-UPV/EHU) - Materials  
Physics Center MPC, Donostia-San Sebastian, Spain.*

<sup>3</sup>*Dipartimento di Fisica “E. Amaldi”,  
Università di Roma Tre, 00146 Roma, Italy.*

<sup>4</sup>*Departament de Física Fonamental, Universitat de Barcelona,  
Diagonal 647, 08028 Barcelona, Spain.*

## Abstract

Studies of liquid water in its supercooled region have led to many insights into the structure and behavior of water. While bulk water freezes at its homogeneous nucleation temperature of approximately 235 K, for protein hydration water, the binding of water molecules to the protein avoids crystallization. Here we study the dynamics of the hydrogen bond (HB) network of a percolating layer of water molecules, comparing measurements of a hydrated globular protein with the results of a coarse-grained model that has been shown to successfully reproduce the properties of hydration water. With dielectric spectroscopy we measure the temperature dependence of the relaxation time of protons charge fluctuations. These fluctuations are associated to the dynamics of the HB network of water molecules adsorbed on the protein surface. With Monte Carlo (MC) simulations and mean-field (MF) calculations we study the dynamics and thermodynamics of the model. In both experimental and model analyses we find two dynamic crossovers: (i) one at about 252 K, and (ii) one at about 181 K. The agreement of the experiments with the model allows us to relate the two crossovers to the presence of two specific heat maxima at ambient pressure. The first is due to fluctuations in the HB formation, and the second, at lower temperature, is due to the cooperative reordering of the HB network.

Recent experiments study water in the first hydration shell of globular proteins [1–5]. Contrary to bulk water, this water does not freeze until the temperature  $T$  is well below 235 K [6], with possibly important implications for biological function [8]. While quasi-elastic neutron scattering investigations [1] and some molecular dynamics simulations [9, 10] support the presence of a dynamic crossover at about 220 K, other experiments and simulations [2–4, 11] do not. It has been shown that the suggested crossover could be related to the anomalous behavior of water, but independent of a possible liquid–liquid critical point at finite  $T$  [12].

Here we show by experiments, simulations, and model calculations that the dynamical properties of the HB network at the protein–water interface exhibit not one, but two dynamic crossovers in the one-phase region at low pressure. We show how the two crossovers are related to the thermodynamics of water. We investigate the dielectric relaxation time of water protons, due to charged defects—such as  $\text{H}_3\text{O}^+$ —moving with a diffusive or hopping mechanism along the HB network [6, 7]. These measurements are a sensitive probe for the HB breaking and formation [13]. We perform dielectric relaxation experiments on lysozyme powder with hydration level  $h = 0.30$  g  $\text{H}_2\text{O}$ /g dry protein, over a broad frequency ( $10^{-2}$  s $^{-1}$  –  $10^8$  s $^{-1}$ ) and temperature range ( $150 \text{ K} \leq T \leq 300 \text{ K}$ ). The experimental set-up and the data analysis [14–18] are described in the Methods section and Supporting Information.

In the dielectric spectrum for lysozyme powder at 215 K, (Fig. 1a), we identify (i) a low frequency tail, (ii) a relatively broad process at intermediate frequency, and (iii) a small high frequency relaxation. The low frequency tail (i) is due to electrode polarization, to interfacial dispersion—also known as Maxwell-Wagner effect—and to sample conductivity (see Methods section). The high-frequency process (iii) has a relaxation time with a  $T$ -dependence and absolute values identical to recent dielectric measurements on the same protein at the same water content  $h$  [3, 4]: this process is labeled as “main” in the above cited literature, and we will adopt this choice (see Methods section and Fig. 1 in the Supporting Information). This relaxation becomes undetectable at hydration levels below  $h \sim 0.3$  g  $\text{H}_2\text{O}$ /g dry protein, and it has been assigned to a local relaxation of protein hydration water [3].

The broad relaxation process (ii), whose width is about 3.5 frequency decades at half maximum, can be resolved into two contributions [14] relatively close in frequency and largely overlapping but with a resulting markedly different  $T$ -dependence (Fig. 2). Such

decomposition has not been discussed in previous work [3, 4, 8], but a quantitative test for the presence of two relaxation processes has been described in detail in Ref. [14] (see Methods section and Supporting Information). The quality of the two-relaxation fit, along with the  $T$ -dependence,  $h$ -dependence, and shape of each relaxation, impels us to conclude that two separate relaxations are present (see Supporting Information). Here we label these processes “side chain” relaxation and “proton” relaxation (Fig. 1). This labeling is based on previous studies on the  $T$ -dependence and  $h$ -dependence of the dielectric response of the same protein and of a similar globular protein (myoglobin). In particular, the “side chain” process has a relaxation time whose  $T$ -dependence and absolute values agree with those measured by others for hydrated lysozyme powders [3] and hydrated myoglobin [8] (see Methods and Fig. 1 in the Supporting Information). The “side chain” relaxation has a symmetric shape over the entire temperature range investigated (see Fig. 3), in agreement with previous findings [3]. This observation provides additional support to distinguish the “side chain” relaxation from the more asymmetric “proton” relaxation. Moreover, the wide temperature and frequency ranges investigated allow to follow these two processes carefully and to identify them even when they are largely overlapping. Fitting parameters for each process, such as its relaxation time and shape parameters, change gradually with temperature, in such a manner to make the distinction between “side chain” and “proton” relaxation reliable at all temperatures.

The “proton” relaxation, contributing to the broad peak in Fig. 1, is the object of the present report and has been extensively studied [6, 14–18] at hydration  $h < 0.30$  g H<sub>2</sub>O/g dry protein. At these hydration levels we find that the “side chain” relaxation is indeed quite small and shows an extremely strong slowing down with dehydration, in agreement with Ref. [3]. The measured dielectric spectra for lysozyme at  $h < 0.30$  g H<sub>2</sub>O/g dry protein is therefore dominated by the “proton” relaxation [6, 14–18]. Its characteristic relaxation time and the related dc conductivity has been described in terms of percolation theory [6, 15]. Its assignment to water-assisted proton displacements over the protein surface has been tested by measuring hydrogenated and deuterated samples [6, 16], and its quantum character has been checked experimentally by dielectric spectroscopy and deep inelastic neutron scattering [16, 19], and verified against theoretical models [20].

At hydration  $h < 0.30$  g H<sub>2</sub>O/g dry protein, the proton relaxation process has a characteristic relaxation time whose temperature dependence is well described by the Vogel-Fulcher-Tamman (VFT) equation  $\tau(T) = \tau_0 \exp[B_T/R(T - T_0)]$ , where  $\tau_0$ ,  $B_T$  and  $T_0$  are

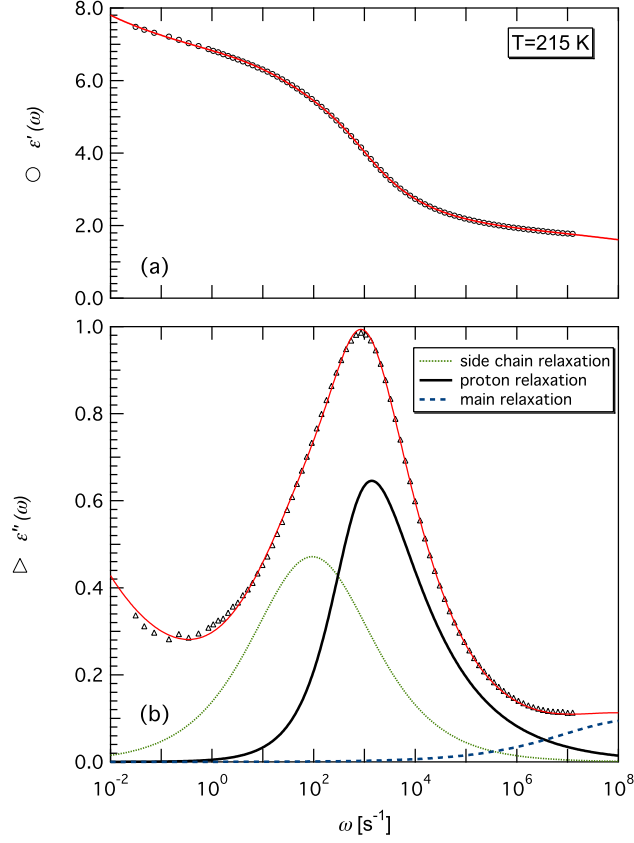


FIG. 1: Dielectric relaxation data for lysozyme powder at 215 K and hydration level  $h = 0.30$  g  $\text{H}_2\text{O}/\text{g}$  dry protein. **(a)**  $\epsilon'$  ( $\circ$ ) and **(b)**  $\epsilon''$  ( $\Delta$ ) are real and imaginary components, respectively, of the complex permittivity  $\epsilon_m^* \equiv \epsilon' - i\epsilon''$ , and  $\omega$  is the angular frequency. Solid lines through symbols result from the fitting procedure in the complex plane [14–18], described in the Method section and Supporting Information. As shown in (b) for  $\epsilon''$ ,  $\epsilon_m^*$  is resolved into (i) a low- $\omega$  tail (omitted for clarity), (ii) a broad process at intermediate  $\omega$  deconvoluted into two relaxations (continuous and dotted lines), and (iii) a high- $\omega$  relaxation (dashed line).

fitting parameters and  $R$  is the gas constant. For the sample water content,  $h = 0.30$  g  $\text{H}_2\text{O}/\text{g}$  dry protein, the proton relaxation time  $\tau$  at high  $T$  shows a VFT behavior, with a clear kink at  $T \approx 252$  K (Fig. 4a), where we find a crossover from one high- $T$  VFT behavior to a second VFT behavior at lower temperature. We associate the crossover at  $\approx 252$  K to a change of the diffusion regime of water protons, from sub-diffusive at lower  $T$  to freely diffusive at higher  $T$ , that has been previously reported for a lysozyme sample at  $h = 0.26$  g  $\text{H}_2\text{O}/\text{g}$  dry protein and 260 K [15]. Interestingly, the VFT description at high temperature

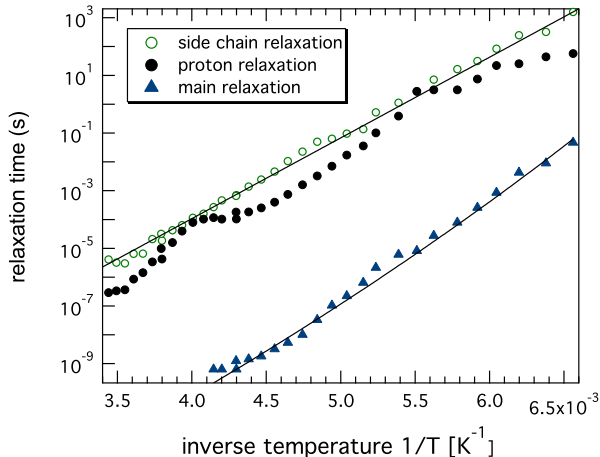


FIG. 2: Temperature dependence of the characteristic times of the relaxation processes shown in Fig. 1: “side chain” relaxation ( $\circ$ ) and “proton” relaxation ( $\bullet$ ) of the intermediate- $\omega$  relaxation (ii), and “main” relaxation ( $\blacktriangle$ ) of the high- $\omega$  relaxation (iii). Solid lines are Arrhenius fits.

of the water proton relaxation time is characterized by the same  $T_0 \sim 200$  K independent of sample hydration [14–16]. Moreover,  $\tau$  would reach 100 s at  $\sim 220$  K (Fig. 4a): this is often defined as the dielectric glass transition temperature. This value is in good agreement with the calorimetric glass transition temperature of the hydrated protein at the same hydration level [3, 4, 13, 15, 17, 18].

At  $T \approx 181$  K we observe a second crossover, as the  $T$ -dependence of  $\tau$  changes from the VFT above 181 K to Arrhenius  $\tau(T) = \tau_0 \exp(A/RT)$  below 181 K, where  $\tau_0$  is a characteristic relaxation time and  $A$  is a constant activation energy (Fig. 4a). The crossover at  $\approx 181$  K, to our knowledge, has never been reported before. Here we offer its possible interpretation based on the results of the model described below: we assign this crossover to a structural rearrangement of the HB network.

It must be noted that neutron scattering experiments on the same hydrated protein also revealed two dynamical transitions, one at 220 K and the other at 150 K [21]. These transitions have been attributed respectively to the rotational motion of interfacial water, and to proton dynamics on a local (few Å) scale. In particular, the low temperature transition (150 K) was claimed to be due to a sudden increase of the configurational entropy of the system, linked to a significant excursion of the HB length [21]. However, deep inelastic neutron scattering experiments on the same hydrated protein do not support this claim, as no

change of the HB length and of the proton potential can be measured up to 290 K [16, 19].

We understand the microscopic mechanisms responsible for the dynamic crossovers observed at 252 K and 181 K, by means of a coarse-grained model of a monolayer of water adsorbed on a generic inert substrate, representing the low-hydrated protein powder. At the hydration level considered here, the adsorption is such that water molecules are restricted to a surface geometry with coordination number up to four [22], and the temperature of their structural arrest is expected to be much higher than 250 K [23], hence they do not diffuse. Yet water molecules do not crystallize [23], therefore, their positions and orientations fluctuate, forming and breaking HBs. These assumptions are grounded on the observation that, at the relatively low  $h$  value investigated, we have less than one monolayer of water molecules covering the protein surface, and the protein itself does not undergo any configurational transformation or large scale motion [6, 23]. This model, originally proposed in Ref. [24] and extensively studied, e. g., in Refs. [12, 25–30], reproduces the known properties of water at interfaces, including the shape of the locus of temperatures of maximum density in the  $(T, P)$  plane, the anomalous behavior of thermodynamic response functions, the subdiffusive regime at low  $T$  for protein hydration water, the occurrence of minima and maxima in diffusivity upon pressurization [31], and has predicted behaviors for protein hydration water, successively verified by experiments [12, 32].

The model discretizes the coordinates of the water molecules in the monolayer into  $N$  cells, each containing one molecule, with a volume given by the inverse of the average water density and a height given by the monolayer thickness. To take into account the change of configurational entropy upon HB formation, the model associates to each molecule  $i$  a variable  $\sigma_{ij} = 1, 2, \dots, q$  with a discrete number of states  $q$  describing the bonding state with a neighbor molecule  $j$ . The model chooses  $q$  by adopting the standard convention that  $30^\circ$  is the maximum deviation of a HB from a linear bond, i.e.  $q \equiv 180^\circ/30^\circ = 6$ . For every molecule there are  $q^4 = 6^4 \equiv 1296$  total possible bonding states. The system is fully specified by the average density  $V/N$  and the set of  $\sigma_{ij}$ .

The model separates the interactions among molecules into three components. The first is the sum of all isotropic interactions (e.g., van der Waals) between molecules at distance  $r \equiv (V/N)^{1/d}$ , and is represented by a Lennard–Jones potential,  $U_0(r) = \epsilon[(r/r_0)^{12} - (r/r_0)^6]$ . On the basis of previous experiments, the model choose attractive energy  $\epsilon = 5.8$  kJ/mol [33] and  $r_0 \equiv (v_0)^{1/d} = 2.9$  Å [34].

The second is the directional component of the HB interaction. Neighboring molecules  $i$  and  $j$  form a HB when their facing bonding variables are in the same state, i.e.  $\sigma_{ij} = \sigma_{ji}$ . Formation of a bond leads to a decrease of local energy by amount  $J = 2.9$  kJ/mol, and an increase of local volume by amount  $v_{\text{HB}}$ . Based on the change of density between tetrahedral ice Ih and interpenetrating tetrahedral network as in ice VI or ice VIII, the model choose  $v_{\text{HB}}/v_0 = 0.5$ . Note that the volume increase  $v_{\text{HB}}$  does not correspond to a larger separation between molecules, but to a larger volume per molecule, due to a decrease of number of neighbors. As a consequence, the increase  $v_{\text{HB}}$  does not affect the  $U_0(r)$  term. The total contribution to the enthalpy is given by  $-(J - Pv_{\text{HB}})N_{\text{HB}}$ , where  $P$  is pressure, and  $N_{\text{HB}}$  is the number of HBs in the system.  $N_{\text{HB}}$  is a function of the configuration of variables  $\sigma_{ij}$

$$N_{\text{HB}} = \sum_{\langle i,j \rangle} \delta_{\sigma_{ij}, \sigma_{ji}} \quad (1)$$

where  $\langle i, j \rangle$  indicates nearest-neighbors, and  $\delta_{a,b} = 1$  if  $a = b$ , else  $\delta_{a,b} = 0$ .

The final interaction is the cooperative (i. e. many-body) interaction among HBs which gives rise to O–O–O correlation [35], locally driving the molecules toward an ordered configuration. This is modeled with an interaction among the four  $\sigma_{ij}$  within the same cell, driving them towards the same state. There is a local energy decrease by an amount  $J_\sigma = 0.29$  kJ/mol for each of the six possible pairs of  $\sigma_{ij}$  within the same cell which are in the same state.

The enthalpy of this model at pressure  $P$  is [24–26]

$$H = \sum_{ij} U_0(r_{ij}) - (J - Pv_{\text{HB}})N_{\text{HB}} - J_\sigma \sum_{(k,l)_i} \delta_{\sigma_{ik}, \sigma_{il}} + PV_0, \quad (2)$$

where the first sum is over all pairs of molecules  $(i, j)$ , the second sum is over all pairs of  $\sigma_{ik}$  belonging to molecule  $i$ , and  $V_0 \geq Nv_0$  is the water volume without counting the contribution of the HBs.

We perform MC simulations at constant  $N = 10^4$ ,  $P$  and  $T$ , where  $V_0$  fluctuates and the configuration of variables  $\sigma_{ij}$ , and therefore  $N_{\text{HB}}$ , changes, resulting in a variable total volume  $V \equiv V_0 + N_{\text{HB}}v_{\text{HB}}$ . We explore the thermodynamics of the system in the  $P$ – $T$  plane, confirming previous results [12, 24–29, 36].

Next, we study the dynamic evolution of the system, by adopting the single-spin flip implemented through the Metropolis algorithm, corresponding to Model A in the classification

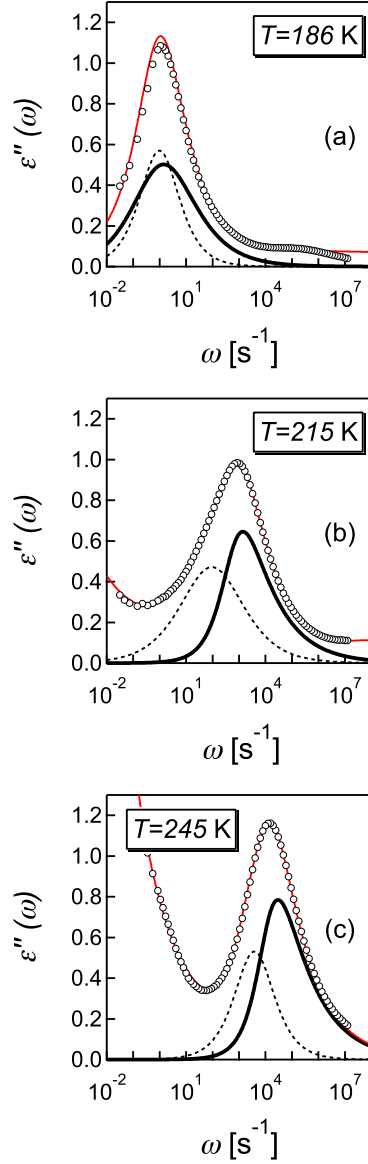


FIG. 3: Imaginary component  $\epsilon''(\omega)$  of the measured complex permittivity as a function the angular frequency  $\omega$ , at three temperatures: (a)  $T = 186$  K, (b)  $T = 215$  K, (c)  $T = 245$  K. Solid lines trough symbols are result of the fitting procedure in the complex plane (see Methods section and Supporting Information). Here we show the results of the decomposition into two processes of the broad relaxation peak. Dashed lines represent the “side chain” relaxation, while thick solid lines represents the “proton” relaxation. The fitting procedure yields a  $\beta_1 \approx 1$  (see Equation 5) for the “side chain” relaxation over the entire temperature range investigated, resulting in a symmetric relaxation process. Conversely, the same procedure gives a  $\beta_2 < 1$  for the “proton” relaxation, resulting in a characteristic asymmetric shape. We omit for clarity the contributions due to sample conductivity and to electrode polarization at low frequency.



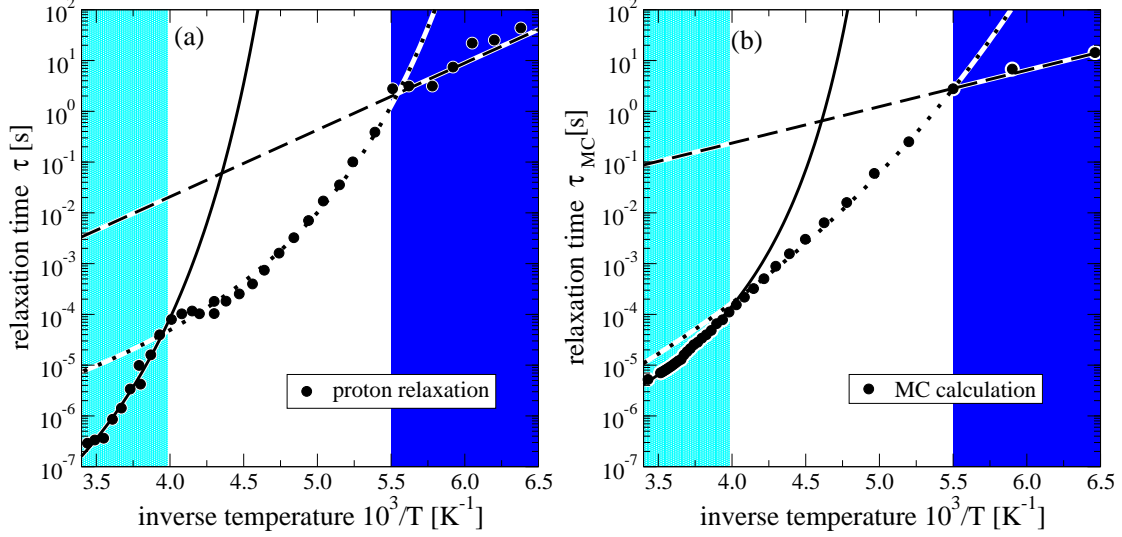


FIG. 4: Two crossovers in the “proton” relaxation time  $\tau$  of hydration water. We find a non-Arrhenius to non-Arrhenius crossover at  $T \approx 252$  K and a non-Arrhenius to Arrhenius crossover at  $T \approx 181$  K. **(a)** Experimental  $\tau$  ( $\bullet$ ) vs.  $1/T$ . Solid line is the VFT function with fitting parameters  $\tau_0 = 7.8 \times 10^{-12}$  s,  $B_T = 9.4$  kJ/mol,  $T_0 = 180$  K. Dotted line is the VFT function with  $\tau_0 = 6.5 \times 10^{-8}$  s,  $B_T = 6.2$  kJ/mol,  $T_0 = 140$  K. Dashed line is the Arrhenius function with fitting parameters  $\tau_0 = 1.1 \times 10^{-7}$  s,  $A = 25.2$  kJ/mol. The behaviors at high and low  $T$  intersect at about 232 K. **(b)** MC relaxation time  $\tau_{MC}$  ( $\bullet$ ) vs.  $1/T$ , for  $P = 0.1$  MPa. Solid line is the VFT function with  $\tau_0 = 1.61 \times 10^{-8}$  s,  $B_T = 5.2$  kJ/mol,  $T_0 = 181.2$  K. Dotted line is the VFT function with  $\tau_0 = 7.5 \times 10^{-10}$  s,  $B_T = 15.9$  kJ/mol,  $T_0 = 95.2$  K. Dashed line is the Arrhenius function with  $\tau_0 = 3.3 \times 10^{-4}$  s,  $A = 13.7$  kJ/mol. See the text for the discussion about the quantitative differences between the numerical and the experimental results.

of Hohenberg and Halperin [37]. The most straightforward quantity to compare with the experiments considered here is the autocorrelation function

$$C_M(t) \equiv \frac{1}{N} \sum_{i=1}^N \frac{\langle M_i(t_0+t)M_i(t_0) \rangle - \langle M_i \rangle^2}{\langle M_i(t_0)^2 \rangle - \langle M_i \rangle^2} \quad (3)$$

where  $t$  is the time measured in MC steps,  $t_0$  is a time larger than the equilibration time of the system,  $M_i \equiv \frac{1}{4} \sum_j \sigma_{ij}$  quantifies the order of the four bond indices  $\sigma_{ij}$  of molecule  $i$ . Defining the MC relaxation time  $\tau_{MC}$  from  $C_M(\tau_{MC}) = 1/e$ , we observe two crossovers in the computed  $\tau_{MC}$ : from VFT to VFT at higher  $T$ , and from VFT to Arrhenius at lower  $T$ . We rescale our experimental data using real units, setting the higher- $T$  crossover at  $T \approx 252$  K

[38] and the lower- $T$  crossover at  $T \approx 181$  K (Fig. 4b) [36]. We find a good agreement of the MC results with the experimental data in Fig. 4, with some difference at high  $T$  that we will discuss in the following. The agreement suggests that the model could provide a good description of the dynamics and connectivity of the real HB network, thus allowing us to use it as a tool to investigate the thermodynamic origin of the observed crossovers.

Next, we discuss the thermodynamic interpretation of the crossover in the model. Reference [12] shows by direct calculations of the model in Eq.(2) that a maximum in isobaric specific heat  $C_P(T) \equiv (\partial H/\partial T)_P$ , implies a crossover in the temperature dependence of  $\tau$ . This result is consistent with the Adam-Gibbs theory [39]. In the present work we find the  $C_P$  maximum observed in Ref. [12], and also another maximum at a lower  $T$ , in a region not explored in Ref. [12] (Fig. 5a). To understand the origin of the two  $C_P$  maxima, we write the enthalpy as the sum of two terms  $H = H^{\text{HB}} + H^{\text{Coop}}$ , where  $H^{\text{HB}} \equiv \langle -(J - Pv_{\text{HB}})N_{\text{HB}} + PV_0 \rangle$ , and  $H^{\text{Coop}} \equiv H - H^{\text{HB}}$ . We define the HB contribution to the specific heat  $C_P^{\text{HB}} \equiv (\partial H^{\text{HB}}/\partial T)_P$ , and the cooperative contribution  $C_P^{\text{Coop}} \equiv (\partial H^{\text{Coop}}/\partial T)_P$ .  $C_P^{\text{HB}}$  is responsible for the broad maximum at higher  $T$  (Fig. 5a). To show that  $C_P^{\text{HB}}$  captures the enthalpy fluctuations due to the HB formation, we calculate the locus of maximum fluctuation of  $\langle N_{\text{HB}} \rangle$ , related to the maximum of  $|d\langle N_{\text{HB}} \rangle/dT|_P$ . The temperatures of these maxima coincide with the locus of maxima of  $C_P^{\text{HB}}$  (Fig. 5b).

The maximum of  $C_P$  at lower  $T$  is given by the maximum of  $C_P^{\text{Coop}}$  (Fig. 5a). To confirm that  $C_P^{\text{Coop}}$  corresponds to the enthalpy fluctuations due to the cooperative  $J_\sigma$ -term in Eq.(2), we calculate  $|d\langle N_{\text{Coop}} \rangle/dT|_P$ , where  $\langle N_{\text{Coop}} \rangle$  is the average number of molecules with perfect local order of their bond indices. We find that the locus of maxima of  $|d\langle N_{\text{Coop}} \rangle/dT|_P$  overlaps with the locus of maxima of  $C_P^{\text{Coop}}$  (Fig. 5b). The same qualitative behavior for  $C_P$  is predicted from MF calculations [29] for the cell model (Fig. 5c).

The non-monotonic behavior of  $\langle N_{\text{HB}} \rangle$  and  $\langle N_{\text{Coop}} \rangle$  explains the two crossovers in the HB correlation time. At very low  $T$ , both experimental  $\tau$  and simulation  $\tau_{\text{MC}}$  have an Arrhenius behavior with constant activation energy  $A$ : 25.2 kJ/mol in the experiments and 13.7 kJ/mol in the model. The quantitative difference between the two arises from the choice of the parameters  $J$  and  $J_\sigma$ . In both experiments and model,  $A$  is consistent with the average energy  $\langle E_{\text{HB}} \rangle$  necessary to break a HB in a locally ordered environment. The relation  $A \approx \langle E_{\text{HB}} \rangle$  in both experiments and model suggests that the dynamics is dominated by the breaking and formation of a single HB at low  $T$ . This is well understood in the model

where the energies  $A \approx \langle E_{\text{HB}} \rangle$  are both functions of  $\langle N_{\text{HB}} \rangle$  and  $\langle N_{\text{Coop}} \rangle$  [12]. Therefore, the saturation of the HB network ( $|\text{d}\langle N_{\text{HB}} \rangle/\text{d}T|_P \approx 0$ ) and its ordering ( $|\text{d}\langle N_{\text{Coop}} \rangle/\text{d}T|_P \approx 0$ ) at low  $T$  imply constant  $A$  and an Arrhenius behavior for the HB correlation time.

At high  $T$  where  $C_P$  is monotonic,  $\langle N_{\text{HB}} \rangle$  and  $\langle N_{\text{Coop}} \rangle$  increase for decreasing  $T$ . Hence, the activation energy and  $\langle E_{\text{HB}} \rangle$  also increase, implying a non-Arrhenius behavior.

At intermediate  $T$ , between the two maxima of  $C_P$ , the rate of change of  $\langle E_{\text{HB}} \rangle$  is proportional to the decreasing  $|\text{d}\langle N_{\text{HB}} \rangle/\text{d}T|_P$  and the increasing  $|\text{d}\langle N_{\text{Coop}} \rangle/\text{d}T|_P$ , giving rise to another non-Arrhenius behavior down to the temperature of the maximum  $|\text{d}\langle N_{\text{Coop}} \rangle/\text{d}T|_P$  and the crossover to Arrhenius behavior [40]. The difficulty to separate the large lysozyme contribution and the low- $h$  water contribution from the total experimental  $C_P$  makes not possible a straightforward comparison of our  $C_P$  calculations with experimental data [21, 23].

The relaxation time calculated for the model is characteristic to the breaking and forming of H bonds, which is analogous to the proton relaxation measured by dielectric spectroscopy. We find good qualitative agreement between  $\tau$  and  $\tau_{\text{MC}}$ , but at high  $T$  the crossover for  $\tau$  is more pronounced than that for  $\tau_{\text{MC}}$  (Fig. 4). This difference arises from two factors.

(i) The experiments are carried out at constant  $h$ , corresponding to a decreasing effective  $P$  (possibly negative due to the surface adsorption) acting on water for decreasing  $T$ , while the MC results are at constant  $P = 0.1$  MPa. Our MF calculations predict that  $C_P$  displays two maxima along any path  $P(T) \lesssim 0.1$  MPa. Along a path such as in the experiments, in which  $P(T)$  decreases monotonically upon cooling,  $\langle E_{\text{HB}} \rangle$  increases more rapidly by decreasing  $T$ , because  $\langle N_{\text{HB}} \rangle$  and  $\langle N_{\text{Coop}} \rangle$  increase more rapidly when both  $P$  and  $T$  decrease [26, 27]. This allows  $\tau_{\text{MC}}$  to converge to the experimental  $\tau$  at high  $T$ .

(ii) The fluctuations in the HB network and distance between water oxygens, predicted by the model, could enhance the probability for a proton to be delocalized between two first-neighbor oxygens, inducing shorter proton relaxation times than those predicted on the base of classical simulations at high  $T$ . Experiments [16] show that this effect is maximum around 250 K, approximately where the model predicts the maximum fluctuation of the HB network and the experimental  $\tau$  shows a stronger cusp than  $\tau_{\text{MC}}$ .

To conclude, in dielectric spectroscopy experiments on hydrated lysozyme at low hydration level, we observe a relaxation mode associated to water protons, with two crossovers: one at  $\approx 252$  K and another at  $\approx 181$  K. At the same time we find that a coarse-grained model of an adsorbed monolayer of water shows in simulations two crossovers for the HB

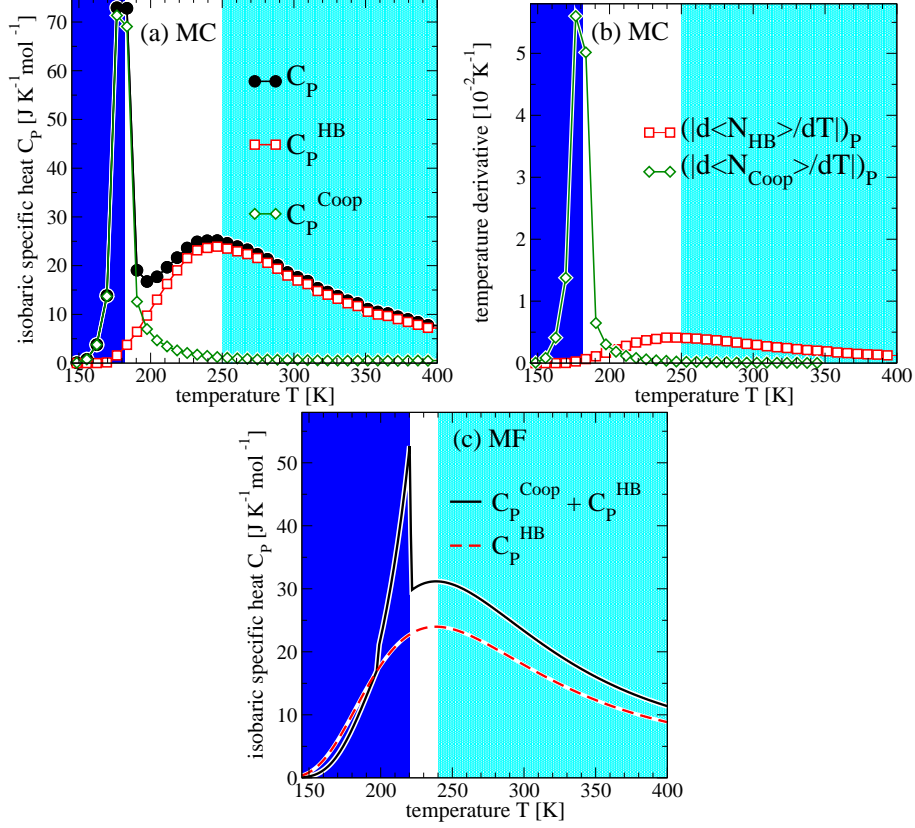


FIG. 5: Two maxima in the specific heat for the model. **(a)** The MC isobaric specific heat  $C_P$  ( $\bullet$ ), at  $P = 0.1$  MPa has two maxima, decomposed into the components  $C_P^{\text{HB}}$  ( $\square$ ) and  $C_P^{\text{Coop}}$  ( $\diamond$ ) described in the text. **(b)**  $|d\langle N_{\text{HB}} \rangle / dT|_P$  ( $\square$ ) and  $|d\langle N_{\text{Coop}} \rangle / dT|_P$  ( $\diamond$ ) show maxima where  $C_P^{\text{HB}}$  and  $C_P^{\text{Coop}}$ , respectively, have maxima. **(c)** MF calculations at  $P = 0$  for the case with cooperative interaction ( $J_\sigma / \epsilon = 0.05$ , continuous line labeled as  $C_P^{\text{Coop}} + C_P^{\text{HB}}$ ) show two maxima for  $C_P$ , while for the case without cooperative interaction ( $J_\sigma = 0$ , dashed line labeled as  $C_P^{\text{HB}}$ ) there is no low- $T$  maximum that, hence, is due to the cooperativity.

dynamics. In the model these two crossovers can be fully understood as the effects of two structural changes of the HB network. These two structural reorganizations are marked by two maxima in  $C_P$ , as well as in the compressibility  $K_T$  and the isobaric thermal expansion coefficient  $\alpha_P$  (not shown here). The two structural changes are (i) at higher  $T$ , associated with the maximum fluctuations of the formation and breaking of the HBs, and (ii) at lower  $T$ , associated with the maximum fluctuation of the ordering of the local arrangement of the HBs. We argue that the model predictions provide an interpretation for our experimental findings.

## METHODS

### Experimental set-up and data analysis

We use an Alpha Analyzer dielectric apparatus (Novocontrol) to study crystallized and highly purified lysozyme powder from chicken egg white (Sigma-Aldrich), dialyzed and lyophilized to set its pH, then re-hydrated [14]. The capacitor containing the sample has blocking electrodes, coated by Teflon with thickness  $\sim 1/40$  of the sample thickness. This choice of thickness eliminates the possibility of artifacts in our raw dielectric data, as discussed in a recent publication [41], and provides a “first check” of the reliability of the data analysis procedure adopted here.

Our measured complex admittance  $Y_m(\omega)$  is directly related to the complex permittivity  $\epsilon_m^*(\omega) = \epsilon'_m(\omega) - j\epsilon''_m(\omega)$  given that

$$\epsilon_m^*(\omega) = \frac{h}{i\omega\epsilon_o S} Y_m(\omega). \quad (4)$$

Here  $i = \sqrt{-1}$ ,  $\epsilon_o$  is the permittivity of free space,  $S$  and  $h$  are respectively the electrode surface area and gap thickness. We extract the true sample permittivity from the measured frequency response by performing a complex function fit procedure that takes into account electrode polarization and capacity—that can be represented by a constant-phase-angle (“CPA”) element—interfacial dispersion, also known as the Maxwell-Wagner effect, along with relaxation processes due to the sample itself. Details about the deconvolution of the data are given in the Supporting Information.

We write the measured complex admittance  $Y_m^*(\omega)$  as

$$Y_m^*(\omega) = \left[ (Y_m^*(\omega))^{-1} + (A(i\omega)^d)_{CPA}^{-1} \right]^{-1} \quad (5)$$

where  $A$  and  $d$  characterize the  $\omega$ -dependent fractal polarization due to the blocking electrode, as in [42], and

$$Y_m^*(\omega) = i\omega\epsilon_o \frac{S}{h} \left[ \epsilon_\infty + \sum_{j=1}^N \frac{\Delta\epsilon_j}{[1 + (i\omega\tau_j)^{\alpha_j}]^{\beta_j}} - \frac{\sigma_0}{i\omega} \right] \quad (6)$$

is the admittance of the sample itself—expressed as a conductivity term plus a combination of Havriliak-Negami functions. Here  $\sigma_0$  is the sample conductivity,  $\epsilon_\infty$  is the high frequency

limit of the permittivity,  $\mathcal{N}$  is the number of relaxation processes (i.e.  $\mathcal{N} = 2$  for the broad peak in Fig. 3),  $\Delta\epsilon_j$  and  $\tau_j$  are the dielectric strength and the relaxation time for the  $j$ th contribution, respectively, and  $\alpha_j$  and  $\beta_j$  characterize the shape of the relaxation time distribution function.

The presence of blocking electrodes eliminates the dc-conductivity across the bulk sample, but not the sample conductivity term Eq.(6), related to local displacement of protons along the protein surface [15]. This sample “local” conductivity has the same temperature dependence as that measured in Ref. [2]. Since the experimental set-up in Ref. [2] does not use blocking electrodes, this observation provides a “second check” for the reliability of our data analysis. The check provides also a verification of our data decomposition, because in Ref. [2] a different deconvolution of the data is used, but the results for the same relaxation mode are the same. See the Supporting Information, section I, for a “third check” of our data analysis.

### **Quantitative analysis of the shape of the relaxation time distribution function**

Raicu [43] has proposed a phenomenological “universal dielectric response” function able to describe a single Debye-like relaxation, such as the Havriliak-Negami (HN) relaxation, combined with interfacial dispersion and electrode polarization. An important result of this work is that a distribution function for the relaxation times in the frequency domain can be directly calculated using parameters appearing in the universal response. We adapt an algorithm [44] to obtain, from raw  $\epsilon_m^*(\omega)$  data, a distribution function in the frequency domain, by means of an inverse Laplace Transform with no *a priori* assumption on the kind and number of relaxation processes. This approach has proven to be a reliable tool to obtain a distribution function of relaxation times [45, 46]. Figure 2 of ref. [14] compares the two distribution functions, one based on a single relaxation, the other with no assumption on the number of relaxation processes, for the data set of hydrated lysozyme powder at 270.4 K and  $h = 0.26$  g H<sub>2</sub>O/g dry protein. The analysis shows that the distribution function derived for a single relaxation process plus the effect of electrode polarization and interfacial dispersion does not totally account for the distribution calculated with no *a priori* assumptions. This implies that one or more additional relaxation processes are required to describe the raw dielectric data. We found that an additional relaxation, is sufficient to completely account

for the calculated distribution function. The addition of a third relaxation term results in unphysical negative  $\Delta\epsilon_i$ , therefore is not considered. We assume that a relatively small increase of water content from 0.26 to 0.3 g H<sub>2</sub>O/g dry protein does not change the results of the approach described above.

## Simulations

We simulate  $N = 10000$  water molecules in the  $NPT$  ensemble. To equilibrate such a large system at about 180 K for 100 sec is a task that cannot be accomplished with molecular dynamics simulations of any detailed model of water. To overcome this problem, we (i) adopt a coarse-grained model, as described in the main text, and (ii) use MC simulations. Depending if we want to study thermodynamic quantities or dynamic quantities, we implement two different MC techniques (see the Supporting Information, section II).

We thank F. Caupin, H. Frauenfelder F. Mallamace, S. Sastry, E. G. Strekalova, for discussions, NSF grants CHE0616489, CHE0911389, CHE098218, and CHE0404673 and MICINN-FEDER (Spain) grant FIS2009-10210 for support.

- 
- [1] Chen S-H, Liu L., Fratini E, Baglioni P, Faraone A & Mamontov E (2006) Observation of fragile-to-strong dynamic crossover in protein hydration water. Proc Natl Acad Sci USA 103:9012-9016.
  - [2] Pawlus S, Khodadadi S & Sokolov A P (2008) Conductivity in Hydrated Proteins: No Signs of the Fragile-to-Strong Crossover. Phys Rev Lett 100:108103 .
  - [3] Khodadadi S, Pawlus S & Sokolov A P (2008) Influence of hydration on protein dynamics: Combining dielectric and neutron scattering spectroscopy data. J Phys Chem B 112:14273.
  - [4] Khodadadi S Pawlus S , Roh J H, Garcia-Sakai V, Mamontov E, Sokolov A P (2008) The origin of the dynamic transition in proteins. J Chem Phys 128:195106.
  - [5] Vogel M (2008) Origins of apparent fragile-to-strong transitions of protein hydration waters. Phys Rev Lett 101:225701.
  - [6] Rupley J A and Careri G (1991) Protein hydration and function. Adv Protein Chem 41:37-172.
  - [7] Capaccioli S, Lucchesi M, Rolla P A, Ruggeri G (1998) Dielectric response analysis of a

- conducting polymer dominated by the hopping charge transport. *J Phys Condens Matter* 10:5595-5617.
- [8] Frauenfelder H, Chen H G, Berendzen J, Fenimore P W, Janssonb H, McMahon B. H., Stroer I R, Swenson J & Young R D, (2009) A unified model of protein dynamics. *Proc Nat Acad Sci USA* 106:5129-5134.
- [9] Kumar P, Yan Z, Xu L, Mazza M G, Buldyrev S V, Chen S-H, Sastry S & Stanley, H. E. (2006) Glass transition in biomolecules and the liquid-liquid critical point of water. *Phys Rev Lett* 97:177802.
- [10] Lagi M, Chu X, Kim C, Mallamace F, Baglioni P & Chen S-H (2008) The Low-Temperature Dynamic Crossover Phenomenon in Protein Hydration Water: Simulations vs Experiments. *J Phys Chem B* 112:1571-1575.
- [11] Vogel M (2009) Temperature-Dependent Mechanisms for the Dynamics of Protein-Hydration Waters: A Molecular Dynamics Simulation Study. *J Phys Chem B* 113:9386.
- [12] Kumar P, Franzese G & Stanley H E (2008) Predictions of dynamic behavior under pressure for two scenarios to explain water anomalies. *Phys Rev Lett* 100:105701.
- [13] Peyrard M (2001) Glass transition in protein hydration water. *Phys Rev E* 64:011109.
- [14] Bruni F and Pagnotta S E (2004) Dielectric investigation of the temperature dependence of the dynamics of a hydrated protein. *Phys Chem Chem Phys* 6:1912-1919.
- [15] Pagnotta S E, Gargana R, Bruni F & Bocedi A (2005) Glassy behavior of a percolative water-protein system. *Phys Rev E* 71:031506.
- [16] Pagnotta S E, Bruni F, Senesi R & Pietropaolo A (2009) Quantum behavior of water protons in protein hydration shell. *Biophys J* 96:1939-1943.
- [17] Pizzitutti F and Bruni F (2001) Glassy dynamics and enzymatic activity of lysozyme. *Phys Rev E* 64:052905.
- [18] Pizzitutti F and Bruni F (2001) Electrode and interfacial polarization in broadband dielectric spectroscopy measurements. *Rev Sci Instrum* 72:2502-2504.
- [19] Senesi R, Pietropaolo A, Bocedi A, Pagnotta S E, and Bruni F (2007) Proton Momentum Distribution in a Protein Hydration Shell. *Phys Rev Lett* 98:138102.
- [20] Tuckerman M E and Marx D (2001) Heavy-Atom Skeleton Quantization and Proton Tunneling in “Intermediate-Barrier” Hydrogen Bonds. *Phys Rev Lett* 86:4946-4949.
- [21] Zanotti J-M, Gibrat G and Bellissent-Funel M-C (2008) Hydration water rotational motion



- as a source of configurational entropy driving protein dynamics. Crossovers at 150 and 220 K. *Phys Chem Chem Phys* 10:4865-4870.
- [22] Merzel F and Smith J C (2002) Is the first hydration shell of lysozyme of higher density than bulk water? *Proc Nat Acad Sci USA* 99:5378-5383.
- [23] Miyazaki Y, Matsuo T & Suga H (2000) Low-Temperature Heat Capacity and Glassy Behavior of Lysozyme Crystal. *J Phys Chem B* 104:8044-8052.
- [24] Franzese G and Stanley H E (2002) Liquid-liquid critical point in a Hamiltonian model for water: analytic solution. *J Phys: Condens Matter* 14:2201-2209.
- [25] G. Franzese, Marqués M I & Stanley H E (2003) Intramolecular coupling as a mechanism for a liquid-liquid phase transition. *Phys Rev E* 67:011103.
- [26] Franzese G and Stanley H E (2007) The Widom line of supercooled water. *J Phys: Condens Matter* 19:205126.
- [27] Kumar P, Franzese G, Stanley H E (2008) Dynamics and thermodynamics of water. *J Phys: Condens Matter* 20:244114.
- [28] Mazza M G, Stokely K, Strelakova E G, Stanley H E & Franzese G (2009) Cluster Monte Carlo and numerical mean field analysis for the water liquid-liquid phase transition. *Comp Phys Comm* 180:497-502.
- [29] Stokely K, Mazza M G, Stanley H E & Franzese G (2010) Effect of hydrogen bond cooperativity on the behavior of water. *Proc Nat Acad Sci USA* 107:1301-1306.
- [30] Strelakova E G, Mazza M G, Stanley H E & Franzese G (2011) Large decrease of fluctuations for supercooled water in hydrophobic nanoconfinement. *Phys Rev Lett* 106:145701.
- [31] de los Santos F, & Franzese G (2011) Understanding diffusion and density anomalies in a coarse-grained model for water between hydrophobic walls. [arXiv:1107.0087v1](https://arxiv.org/abs/1107.0087v1).
- [32] Franzese G, Stokely K, Chu X Q, Kumar P, Mazza M G, Chen S H & Stanley H E (2008) Pressure effects in supercooled water: comparison between a 2D model of water and experiments for surface water on a protein. *J Phys: Condens Matter* 20:494210.
- [33] Henry M (2002) Nonempirical quantification of molecular interactions in supramolecular assemblies. *Chem Phys Chem* 3:561-569.
- [34] Narten A H, Danford M D, and Levy H A (1967) X-Ray diffraction study of liquid water in the temperature range 4-200°C. *Faraday Discuss* 43:97-97.
- [35] Ricci M A, Bruni F and Giuliani A (2009) "Similarities" between confined and supercooled

- water. Faraday Discussions 141:347-358.
- [36] To compare with experiments, MC  $T$  is offset of 134.5 K, MC  $P$  is rescaled by 0.507 and offset of  $-2 \times 10^{-4}$  GPa.
- [37] Hohenberg P C, Halperin B I (1977) Theory of dynamic critical phenomena. Rev Mod Phys 49:435-479.
- [38] In [12] this crossover was estimated as VFT to Arrhenius due to the limited resolution at low  $T$ .
- [39] Adam G and Gibbs J H (1965) On the temperature dependence of cooperative relaxation properties in glass-forming liquids. J Chem Phys 43:139-139.
- [40] In the model there is no water diffusion, hence the low- $T$  crossover is not due to a bulk glass transition as hypothesized for fully hydrated cases in Ngai KL, Capaccioli S & Shinyashiki N (2008) The protein “Glass” transition and the role of the solvent. J Phys Chem B 112:3826.
- [41] Richert R (2009) Insulated electrodes for eliminating conductivity in dielectric relaxation experiments. Eur Phys J B 68:197-200.
- [42] Feldman Y, Nigmatullin R, Polygalov E, & Texter J (1998) Fractal-polarization correction in time domain dielectric spectroscopy. Phys Rev E 58:7561-7565.
- [43] Raicu V (1999) Dielectric dispersion of biological matter: Model combining Debye-type and “universal” responses. Phys Rev E 60:4677-4680.
- [44] Provencher S W (1982) A constrained regularization method for inverting data represented by linear algebraic or integral equations. Comput Phys Comm 27:213-227.
- [45] Alvarez F, Alegria A, and Colmenero J (1991) Relationship between the time-domain Kohlrausch-Williams-Watts and frequency-domain Havriliak-Negami relaxation functions. Phys Rev B 44:7306-7312.
- [46] Banys J, Kinka M, Meskauskas A, Macutkevicius J, Vlkel G, Bhlman W, Umamaheswari V, Hartmann M, Pöpl A (2005) Broadband Dielectric Spectroscopy of Water Confined in MCM-41 Molecular Sieve Material. Ferroelectrics 318:201-207.